Journal of Computers Vol. 34 No. 1, February 2023, pp. 117-130
doi: 10.53106/199115992023023401009

Intelligent Tumor Cell Detection Method Based on Circulating Tumor Cell (CTC) Technology

Zhen-Ning Wu, Hao-Sen Huang, Jun-Jun Jiang, Zhong-Zhe Xiao, Min Huang*

School of Optoelectronic Science and Engineering, Soochow University, Jiangsu, China
{znwuznwu, 20204239028, jjjiang1996}@stu.suda.edu.cn; {xiaozhongzhe, hmin}@suda.edu.cn

Received 12 April 2022; Revised 25 August 2022; Accepted 19 September 2022

Abstract. Cancer has become one of the greatest threats for human life. Doctors can get original images of the sick organs with the assistance of medical technology. However, manual interpretation of the original images is time consuming and labor consuming. Nowadays, the intelligent detection of tumor cell images is commonly adopted in cancer diagnosis. In this paper, we propose Imporved Selective Search (ISS) algorithm and CTCNet based on Circulating Tumor Cell (CTC) technology to improve the cancer images' detection efficiency. CTCs can be collected by a sampling needle with EpCAM antibody which can specifically bind to tumor cells. After fluorescent staining process, images obtained from sampling needle will be processed by the ISS algorithm for candidate region preselection. All of the eligible areas are evaluated with a self-designed neural network called CTCNet, resulting in efficient recognition of circulating tumor cells. During this process, all algorithms are accelerated through the GPU and NPU hardware platform, which further improves the detection speed of the system. In the experiment, we first verify the efficiency of proposed ISS algorithm by compared with Original Selective Search (OSS), we found that the number of candidate boxes reduced from 549 to 16 and the time consuming reduced by 0.3s after adopting the ISS algorithm. In order to evaluate the performance of the proposed 7-layer CTCNet, we compared CTCNet with SVM, BP neural network, AlexNet and VGGNet by using the dataset of 12312 samples from 30 patients, among them, there were 12 patients with early cancer and 18 patients with advanced cancer. And we got the highest recognition accuracy of 97.95% on CTCNet, which even beyond the VGGNet with deeper layers. In contrast to other combinations, we detect CTC in diverse clinical CTC images, the joint application of ISS algorithm and CTCNet achieves an outstanding system performance with accuracy up to 94.03% in the whole view images. Meanwhile, because of the application of a lightweight network in different hardware acceleration platform, the detection time of the CTC image in a single view can be less than 12s.

Keywords: circulating tumor cell, tumor cell detection, improved selective-search, convolutional neural network

1 Introduction

Tumor-related diseases have become one of the greatest threats for the security of human life. Therefore, it is imperative to detect tumors for auxiliary diagnosis, which can greatly increase the probability of patients survival. Doctors can get original data (normal images) of the sick organs with the assistance of medical technology such as MRI (Magnetic Resonance Imaging) and CT (Computed Tomography). However, the final diagnosis results deduced from these original data relies greatly on experience and even can be influenced by the state of the doctors in some scenarios. Furthermore, some tumor cell biomarkers, such as CTC (Circulating Tumor Cell), can generate huge amounts of data. Manual identification is very time-consuming and unreliable. In this paper, a novel intelligent tumor cell detection algorithm based on CTC is proposed to provide an efficient and accurate way for tumor cell detection.

Some markers that can be used for tumor detection, including Carcino-Embryonic Antigen (CEA) [1-2], Carbohydrate Antigen (CA) [3], and Alpha Fetoprotein (AFP) [4], have been widely adopted by hospitals as the auxiliary diagnosis, but since these methods lack of specificity, we cannot quantify the metastasis and prognosis of cancer. CTC technology, as a method to label and capture tumor cells specially, has high tumor detection accuracy and can be used in cancer auxiliary diagnosis and cancer metastatic evaluation [5-6].

Most tumor detection methods, including CTC, derive the final diagnosis through their medical images. Image

* Corresponding Author

processing methods like threshold segmentation [7], clustering [8], and morphological and regional analysis [9], [10] are widely adopted to identity tumor cells/tissues. Thanks to the development of machine learning, some more efficient methods, including SVM (Support Vector Machine) [11], BP neural network [12] and deep neural network [13-16], have been applied to tumor cell image recognition.

For CTC, the cell image is captured by a fluorescence-based automated microscope system [17-18]. So far, CTC detection use machine learning mainly based on extracted features [19-22]. These methods take advantage of image features, such as gray scale, color, and morphology. Based on these features, targets can be screened out by a classifier. Once processing CTC in the whole image, features of the image are changed with the inconsistent lighting between equipment and the heterogeneity of tumor cell. This means that CTC detection methods based on feature extraction and traditional machine learning are very vulnerable to the change of imaging system and lack adaptive capabilities in heterogeneous cell regimes.

Because the traditional methods have poor generalization ability for heterogeneous CTCs, we use the deep learning methods for CTC detection. The application of deep learning methods [23-25] has improved the accuracy of CTC images recognition. But they focus more on optimizing network to improve the recognition rate on their datasets. In actual scene, the whole image needs to be detected, and the acquisition of candidate regions affects the performance of the network. We need a candidate region extraction method with strong generalization ability. At the same time, with the application of the deep network, the requirements of the hardware platform for running algorithms are becoming higher and higher [26-27]. Convolutional neural network (CNN) like AlexNet, VGGNet and ResNet are widely used in CTC detection, which increases the computational burden. A reasonable structure is more useful than a deeper network.

According to the analysis of the shortcomings of the traditional image processing methods and the deep learning methods, this paper proposes an intelligent tumor cell detection method. Our research direction is attempted to find a region extracted method with strong generalization ability, and design a lightweight network can realize accurate and quick detection of CTCs. By combining traditional image processing methods and the original selective-search algorithm, an improved selective-search algorithm is proposed, which can efficiently extract the candidate areas in the whole image. Compared with original selective-search algorithm, its selection accuracy has improved several times, and the time consumption has also reduced by 0.3 seconds. A 7-layer convolutional neural network called CTCNet is built for final recognition, experimental results show that CTCNet not only achieves better performance than other deep neural networks, but also decreases the training time. The joint application of ISS algorithm and CTCNet achieves an outstanding performance with accuracy up to 94.03% in the detection of clinical whole field images.

The rest of this paper is organized as follows. Section II discusses the background technology of this paper, including the principle of the CTC sampling needle and the introduction of the neural network. Section III presents the ISS algorithm and the construction of the convolution neural network. Section IV sets up several experiments and presents experimental results. Finally, in Section V, we conclude the paper and describe future work.

2 Background

2.1 The Principles of CTC

The concept of CTC was first induced by Australian doctor Ashworth in 1869. CTC refers to tumor cells proliferating from the primary or metastatic site to the secondary metastasis. Some tumor cells have to invade the vein and enter into the blood circulation system to complete the proliferation process. This provides the opportunity to get more detailed information of the tumor cell through specific blood collection.

We adopt a sampling needle produced by Gilupi, the functional part in which has some active substances and can capture tumor cells in the blood. The collection efficiency is generally higher than normal clinical methods.

CTC can be captured by the functional area of the sampling needle through an upper limb elbow venipuncture within 30 minutes. As shown in Fig. 1, the functional area's 20mm long gold-coated tip contains the antibody to EpCAM, which can accurately recognize target cells with EpCAM on the surface. The hydrogel of the functional area's surface will then 'grasp' target cells. Finally, tumor cells with EpCAM adhere to the surface of the functional area. Different from collecting blood directly, we collect CTCs in vivo. The sampling needle will be left in the vein for 30 minutes and the blood volume we detected is more than 1500ml. With the specific binding of CTCs and EpCAM, the CTC detection rate can reach 80% in cancer patients.

Due to the specificity of the sampling method, it can detect the CTC of lung cancer, breast cancer, colorectal cancer, prostate cancer and bladder cancer. Gold coating and hydrogel coating can effectively prevent non-specif-

ic binding of leukocytes, which ensure the high specificity and purity of the captured CTC. Once tumor cells are captured, the sampling needle can be taken out for fluorescence staining, and the dyed sample is imaged by the microscopic system.

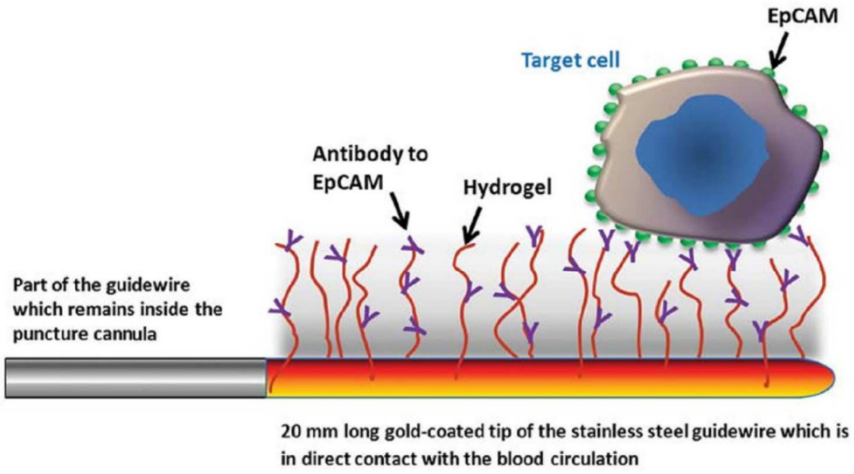

Fig. 1. How EpCAM specifically capture the CTC

2.2 Fluorescence Staining Method and Criteria for the CTC Recognition

During the staining process, different proteins of the cells on the surface of the sampling needle are stained with fluorescence by specific staining reagents with different colors. Tumor circulating epithelial cells, white blood cells and nucleus are stained with green, red and blue respectively. Images of three channels (Red, Green, Blue) as well as the integrated result of these channels can be obtained with different lights of the microscopic system.

Fig. 2 shows typical results of the clinic CTC test. We can observe that the fluorescence expression of normal white blood cells is red and they have no fluorescence expression in green, compared to the tumor cells. Therefore, fluorescence color expressions of Nuclear+, EpCAM/CKs+, and CD45- are utilized as the basic criteria for identifying tumor cells. Some morphological characteristics (such as diameter and areas) are also adopted by the CTC extracted algorithm to further improve its accuracy.

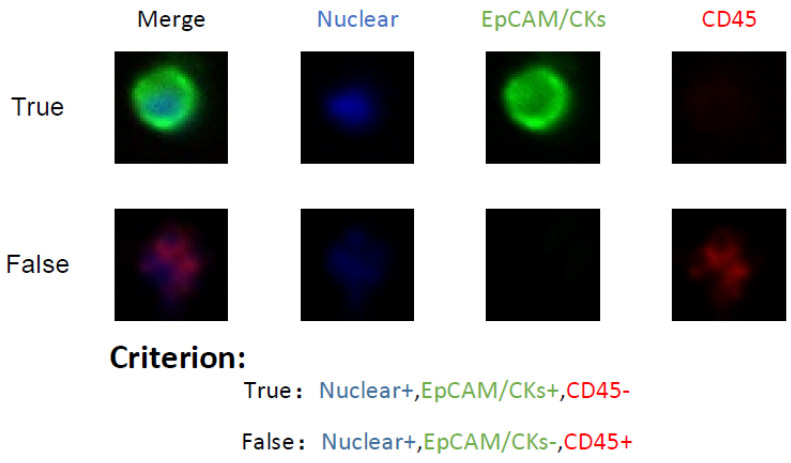

Fig. 2. Criterion of the tumor cell and normal cell

When detecting CTC in the whole image with diversity background, we not only need to consider the features of a single cell, but also have to solve the color inconsistency caused by lighting and the heterogeneity between cells. Due to the difference of imaging system, the color intensity of different images is various, which makes it difficult to judge color information with fixed standards. The heterogeneity of cells leads to some differences in cell morphology, size and color intensity. It is critical to find an effective method to screen and judge these cells. A generalized region selection method and convolution neural network are necessary.

2.3 Overview of Neural Network

Complex connections between neurons and the layers give the network the capability to model high dimensional expressions, which enables comprehensive classification or regression tasks. The convolutional neural network (CNN), which is s typical deep learning network structure, has become the basic tool for the target recognition.

R-CNN is a network improved from the basic convolutional neural network, in which AlexNet is adopted as the main structure of the network, Selective Search is adopted to generate candidate region. It has achieved relatively good performance in cancer image recognition [28-29]. This paper is mainly inspired by the principle of R-CNN, and our proposed detection algorithm is based on some of its basic principles.

3 ISS and CTCNet

To improve the performance of the CTC detection, this paper proposes ISS and CTCNet. As shown in Fig. 3, CTC images can be collected after fluorescent staining and the formation process. Improved Selective Search (ISS) is adopted to preliminary extract all of the cells in the original image and format them into fix sizes. The formatted cell images are sent into CTCNet, which completes the CTC recolonization. In the following subsections, we will present the Improved Selective Search algorithm and the details of CTCNet. In the following subsections, we will present the Improved Selective Search algorithm and the details of CTCNet.

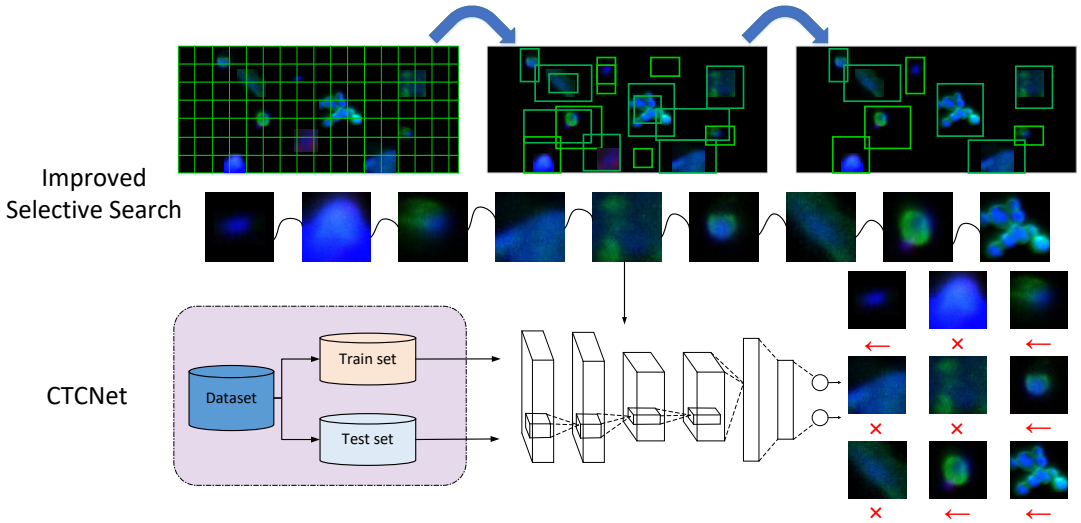

Fig. 3. Algorithm flow

3.1 Improved Selective Search Algorithm

Selective Search is a region proposal algorithm used in object detection. It is designed to be used in fast target detection with a very high recall rate. By using Selective Search to extract the target region, the parts that need to be detected in the image can be quickly found, which avoids traversal of the whole image. In this paper, we propose Improved Selective Search (ISS), which uses similarity of regions to merge and select regions from images. In Improved Selective Search, similarity of regions can be calculated using color, texture, size and shape compatibility. These broad features ensure the generalization ability of the region extraction algorithm.

Color similarity of two regions is based on histogram intersection and can be calculated by:

$$S_{color}(r_i, r_j) = \sum_{k=1}^{n} \min(c_i^k, c_j^k). \tag{1}$$

where c_i^k is the histogram value for k^{th} bin in color descriptor. Texture similarity of two regions is also calculated using histogram intersections:

$$S_{texture}(r_i, r_j) = \sum_{k=1}^{n} \min(t_i^k, t_j^k). \tag{2}$$

where t_i^k is the histogram value for k^{th} bin in texture descriptor. Size similarity is defined as:

$$s_{size}(r_i, r_j) = 1 - \frac{size(r_i) + size(r_j)}{size(im)}. \tag{3}$$

where $size(im)$ is size of image in pixels. Shape compatibility is defined as:

$$s_{fill}(r_i, r_j) = 1 - \frac{size(BB_{ij}) - size(r_i) - size(r_j)}{size(im)}. \tag{4}$$

where $size(BB_{ij})$ is a bounding box around (r_i) and (r_j).

The original Selective Search algorithm are mostly used for target selecting, which may generate a huge amount of candidate boxes, inducing a great burden for the target recognition portion of the network. By limiting the size of the output box, the number of candidate regions can be greatly reduced. However, some cells with a large size or some adhesion cells will be missing.

To further reduce the number of candidate regions while avoiding the missing target problem, the ISS algorithm was proposed. The algorithm flow is shown in Fig. 4.

The input of ISS is the resultant image after staining, and the output is a limited number of suspected CTCs with certain characteristics. The basic idea of ISS is to meet the needs of tumor cell image detection in this paper. Firstly, we set the range of candidate box size to be wide enough (generally 200 pixels to 10000 pixels in area) to take into account all probable regions, which reduces the number of detection regions while improving detection precision.

In order to further reduce the target area, we remove small areas covered by large areas. Next, we use classic image processing methods to filter the candidate regions through color and morphological characteristics, the R, G and B channel graphs of the remaining regions are grayed, then gray-stretched, threshold segmentation is performed, and connected component analysis is done. The results are synthesized according to certain rules: the areas with signal in the blue and green channels and without signal in red channel are made white. Since the selected candidate boxes are of different sizes, we limit all of the selected areas to the same size, 40 × 40, which is a suitable box size for capturing a cell. After the above operations, not only are the number of candidate boxes reduced, but the input image size of the convolutional neural network is also fixed, which greatly reduces the requirements of the network, and at the same time helps to improve the detection efficiency.

Compared with screening in the whole image directly, this not only avoids the interference caused by noise in the background region, but also effectively avoids the direct interference between different regions, so that the detection accuracy is improved naturally. The improvement results of ISS will be presented in the experimental part.

Input: Resultant image after staining.
Output: A limited number of suspected CTCs with certain characteristics.

Divide the initial set of small regions $A = \{a_1, \cdots, a_n\}$.
Define a similarity set $B = \emptyset$.
Define lower limit of the regions'area M
Define upper limit of the regions'area N
for Each neighbouring region pair(a_i, a_j) **do**
    Calculate similarity $b\,(a_i, a_j)$
    $B = B \cup b\,(b_i, b_j)$
end for
while $B \neq \emptyset$ **do**
    Get highest similarity $s\,(a_i, a_j) = \max(B)$
    Merge corresponding regions $a_t = a_i \cup r_j$
    Remove similarities regardinga_i : $B = B \backslash b\,(a_i, a_*)$
    Remove similarities regardinga_j : $B = B \backslash b\,(a_*, a_j)$
    Calculate similarity setB_t between $a_t$and its neighbours
    $B = B \cup B_t$
    $A = A \cup a_t$
end while
for all areas in A **do**
    if $N < area < M$ **then**
        Extract the area from all regions in A
        Remove overlapping areas
        Remove interference areas according to color and morphological characteristics
        Limit the area to a fixed size
    end if
end for

Fig. 4. ISS algorithm

3.2 CTCNet

The network we use for CTC recognition is called CTCNet, which is a convolutional neural network consisting of two convolution layers, two pooling layers, two fully connected layers and a Softmax layer. We use a Rectified Linear Unit (ReLU) as the activation function, which successfully solves the gradient diffusion problem of the sigmoid function. In addition, a Dropout operation is carried out to avoid overfitting of the model. Our network has 7 layers, which not only ensures detection accuracy of the model, but also reduces the training time. CTCNet plays an important role in improving the running speed of algorithm. Fig. 5 shows its structure.

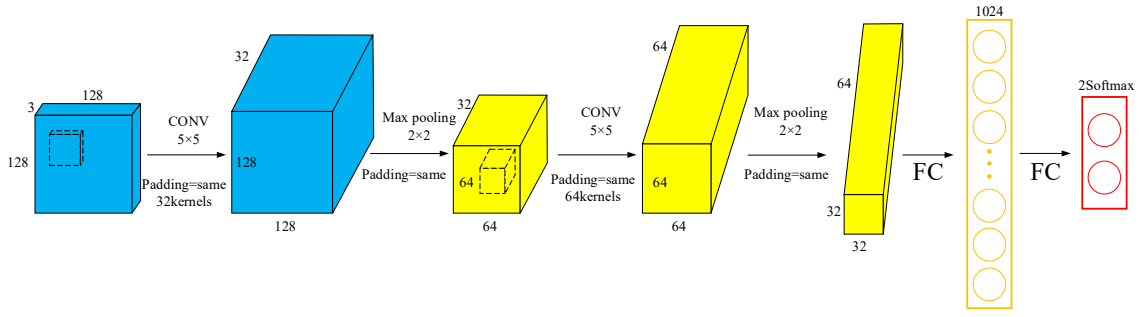

Fig. 5. The structure of the CTCNet

For each convolution layer, the convolution kernel size is set as 5 × 5, during the slide of the convolution kernel, the edge of the image is filled with 0, ReLU is adopted as the activation function. The depth of convolutional layer 1 is 32, and the depth of convolutional layer 2 is 64. The pooling kernel of each pooling layer is 2 × 2 by max- pooling. Two fully connected layers have 1024 and 256 neurons, and the activation function of the fully connected layer is a sigmoid function. The Softmax layer has 2 neurons. To prevent over-fitting, we place a dropout operation with a dropout factor of 0.5 between the fully connected layer and the Softmax layer. The final classification result is output through the Softmax layer.

We set up a dataset for training the convolutional neural network. We separate the data into two folders with true and false labels. The true folder contains positive samples of tumor cell images, and the false folder contains negative samples of normal tumor images or other interference images. The number of positive samples is 573, the number of negative samples is 966. Through three times 90 degrees counterclockwise rotation and mirror the rotated images to extend data set, a data set including 12312 samples is obtained. Since the size of the candidate box is fixed, the size of the sample is set to 40 × 40 too. We present part of the dataset as follow in Fig. 6.

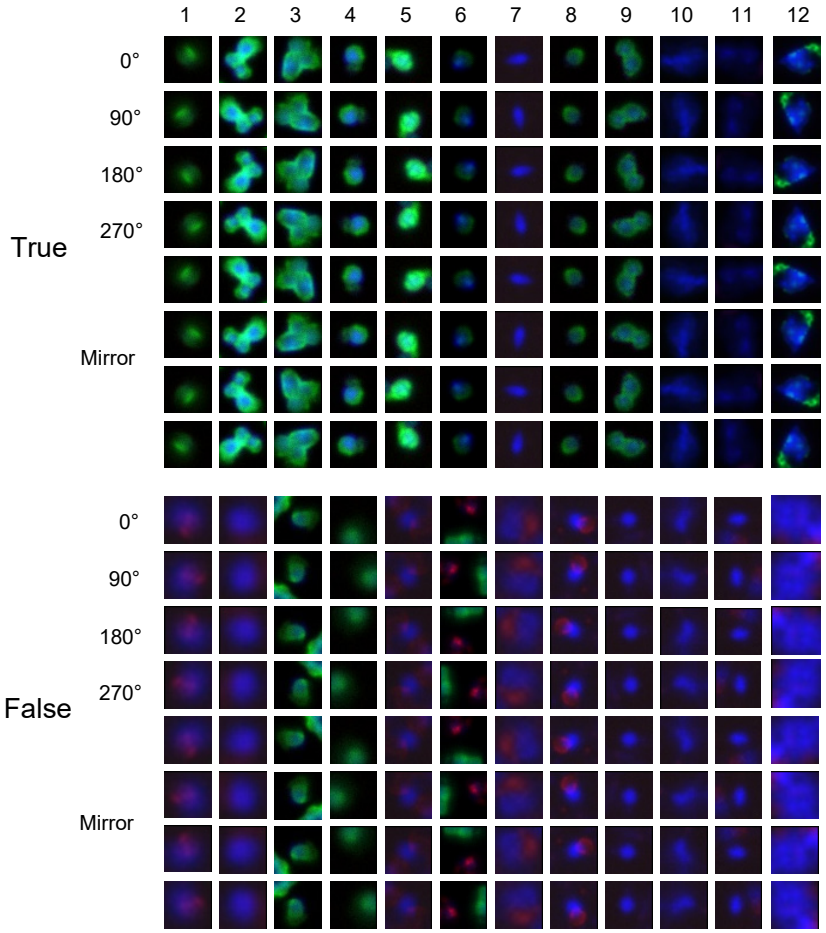

Fig. 6. Partial dataset

When using this dataset for training, 1000 and 2000 epochs are used. Every 50 epochs, the training parameters of the model are stored, and the cross entropy is used as the loss function. The learning rate is 0.05. In the actual detection, the model parameters obtained from training can be loaded directly for test data.

4 Evaluation

We conducted a set of experiments to evaluate the performance of the proposed method in this paper. The method we proposed contain two stages, in candidate region preselection stage, the proposed ISS algorithm was compared

with the original selective search (OSS) algorithm, the method of limiting area size, and the method of relaxing regional restrictions, in terms of the number of candidate boxes and running time of each algorithm. In detection stage, since we are trying to find an efficient method for tumor cell recognition, we designed a lightweight network as shown in Fig. 5. It was evaluated by comparing with SVM, BP, AlexNet and VGGNet. We also combined different region preselection and recognition methods to evaluate the accuracy performance of ISS+CTCNet. To further evaluate the efficiency of the algorithm, we implemented the presented algorithm on different hardware platforms (CPU/GPU/NPU). The NPU platform is a Huawei Ascend Atlas 200 with the Da Vinci architecture. The other platform adopted in the experiment is a Dell workstation with the following configuration:

· Intel i7-8700 CPU
· 16GB DDR4 memory
· NVIDIA Geforce GTX2060Ti GPU

4.1 Experimental Results

To evaluate the effectiveness of the proposed ISS, we compare ISS with Original Selective-Search (OSS) with different configurations. As shown in Table 1 and Fig. 7(a), OSS obviously generates too many valid/invalid candidate boxes. That puts a number of extra invalid candidates into the detection network and wastes a lot of time. The number of extra invalid candidate boxes can be sharply reduced by adding a limitation on the size of candidate boxes, as shown in Fig. 7(b) and Fig. 7(c). However, there are still some invalid candidate boxes that cannot be eliminated only by adjusting the size of candidate boxes.

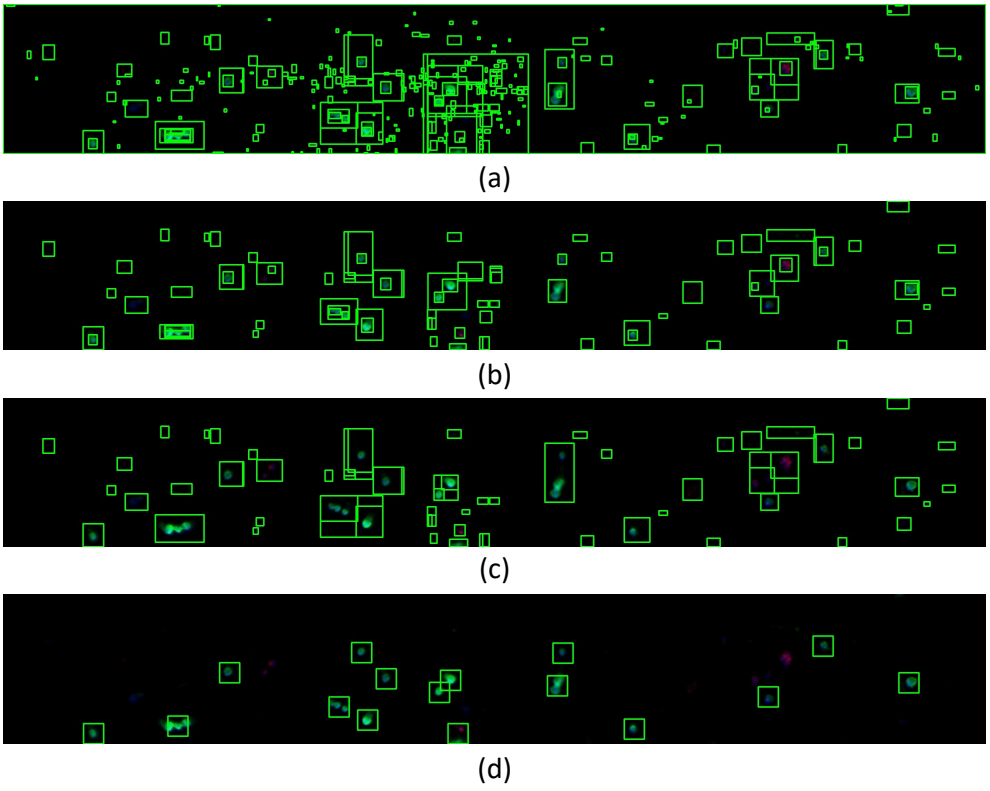

Fig. 7. ISS with Original Selective-Search (OSS) with different configurations
(a) The result of OSS. (b) The result of OSS with candidate box size 10 × 20 to 100 × 100. (c) The result of OSS with candidate box size 10 × 20 to 100 × 100 and overlapping region limitation. (d) The result of ISS algorithm with candidate box size 40 × 40

To further reduce the number of invalid candidate boxes, ISS adopted area size limitation, overlapping area elimination, color feature selection and candidate box size fixing techniques. As shown in Fig. 7(d), the number of candidate boxes is reduced to 16 by adopting the proposed ISS, while the time consumed is almost the same as that of other methods. This means that ISS can effectively reduce the number of candidate boxes with little

overhead. Moreover, the size of the candidate box is the same as that of the training image. That avoids the resize operation, which further improves the accuracy of the network.

Table 1. The performance of above methods compared with ISS

Method	Candidate box numbers	Time consuming (s)
a	549	10.58
b	116	10.95
c	66	8.00
d	16	10.28

In the experiment, we also evaluate the performance of the CTCNet with real clinical image samples. CTC detection technology we used can detect breast cancer, lung cancer and prostate cancer. It can capture CTCs at early and advanced stage, detection rate can reach 60% at early stage. The data set we used is CTC images of 12 patients with early cancer and 18 patients with advanced cancer, including 16 female breast cancer patients and 14 male prostate cancer patients. A total of 4584 positive samples and 7728 negative samples are employed in the training of the network. The training set and the test set is divided by 7 to 3. As shown in Table 2, the following performance metrics are proposed: the accuracy, precision, recall, and F1 score to measure true and predicted classes which have already been represented in equations respectively.

$$Accuracy = \frac{TP + TN}{TP + FN + FP + TN}. \tag{5}$$

$$Precision = \frac{TP}{TP + FP}. \tag{6}$$

$$Recall = \frac{TP}{TP + FN}. \tag{7}$$

$$F1 = 2 \times \frac{Precision \times Recall}{Precision + Recall}. \tag{8}$$

Here TP describes true positive, TN represents true negative, FP indicates to false positive, and FN denotes false negative.

In Table 2, as a lightweight network, CTCNet has even achieved a little better performance than deep network. Based on the dataset of CTC images, CTCNet is the most efficient. To further test the proposed ISS and CTCNet in real scene, we adopted the Classical Image Processing (CIP) method, CIP+BP, CIP+SVM, CIP+AlexNet, OSS+AlexNet(R-CNN), ISS+AlexNet, CIP+VGGNet, ISS+VGGNet, CIP+CTCNet, OSS+CTCNet for comparison. CIP processes the R, G, and B channels of the CTC image separately. Gray stretch, threshold segmentation, three-channel synthesis, and connected domain analysis for the channels after graying are utilized to get the preselected regions or feature vector of CTC cells.

Table 2. The performance of different machine learning methods

Method	TP	TN	FP	FN	Accuracy	Precision	Recall	F1
SVM	29.56	56.63	6.13	7.67	86.19	82.82	79.4	81.08
BP	28.38	52.79	9.97	8.85	81.17	74	76.23	75.1
AlexNet	36.45	59.19	3.57	0.78	95.64	91.08	97.9	94.37
VGG	37.05	60.83	1.93	0.18	**97.88**	95.05	**99.52**	97.23
CTCNet	36.95	61	1.76	0.28	**97.95**	**95.45**	**99.25**	**97.31**

In order to intuitively show the training process of CTCNet, we visualized its training curve in Fig. 8 and plotted the confusion matrix in Fig. 9. It can be seen from the curve that the accuracy on the training set and the test set increased steadily and can reach 97.95%. Due to the setting of the learning rate is a bit high, there will be vibration during the decline of the loss curve, with the increase of training epochs, the loss curve also shows a downtrend. In the confusion matrix, TP and TN are both more than 97%. When we use a simple network, we greatly reduce the training overhead and achieve an accuracy that is not inferior to the complex networks, which indicates that the structural improvement of CTCNet is effective.

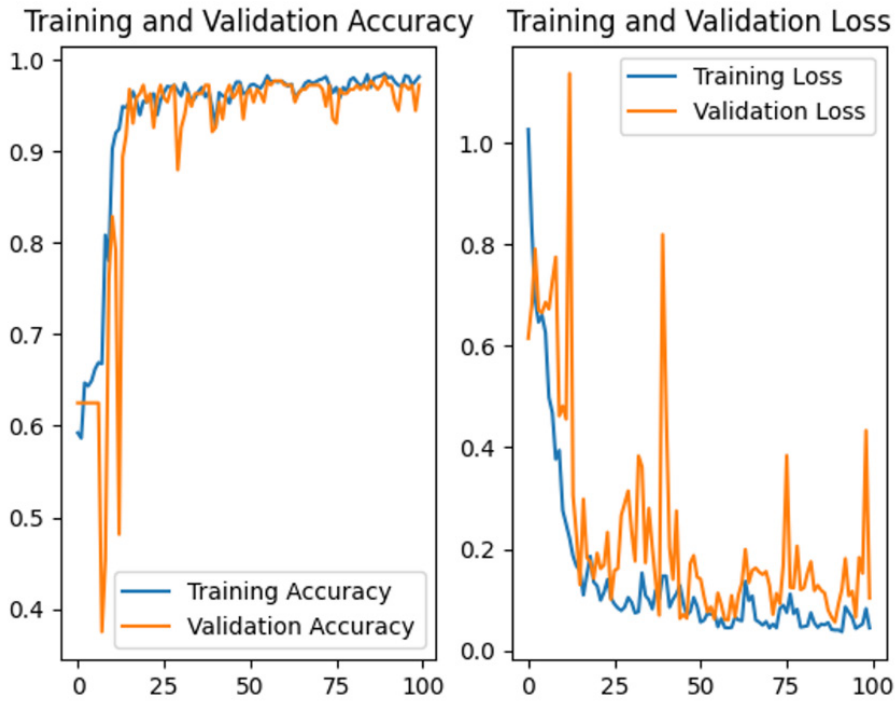

Fig. 8. Accuracy and loss curve of CTCNet

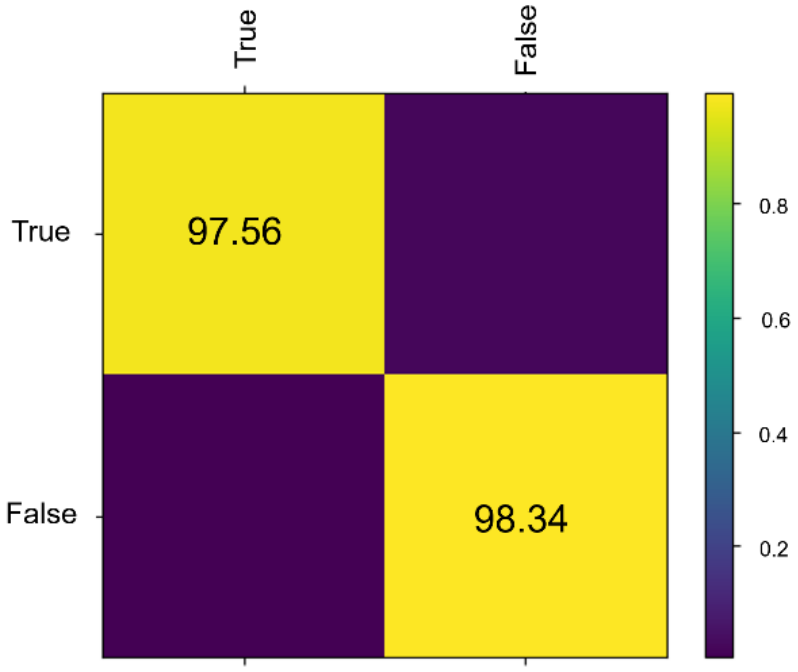

Fig. 9. Confusion matrix of CTCNet

Table 3 shows the test result on clinical images. Although the methods use CIP has excellent speed performance, but its accuracy performance is not well. CIP greatly relies on threshold setting and cannot be adopted for different scenarios with different interference. For example, an unclear background would lead to mismatch of CTC cell targets. However, the parameters of LED lights usually fluctuate with different microimaging systems. This leads to slight differences between captured images, which introduces different types of interfere into captured images. Thus, CIP cannot be easily used in realistic scenarios of CTC detection.

However, it is obvious in Table 3, the accuracy performance of the proposed method is greatly improved compared with CIP method. Through the comparison with deeper network AlexNet and VGGNet, which proves that the use of shallow network CTCNet can also ensure the detection result with the less time consumption. At the same time, by connected with AlexNet, VGGNet and AlexNet, respectively. We can see the good performance of the ISS.

Table 3. The performance of different machine learning methods

Method	Accuracy performance	Speed performance(s)		
		CPU	GPU	NPU
CIP	44.17	**4.66**	**4.28**	**4.16**
CIP+SVM	79.51	6.34	5.88	-
CIP+BP	77.34	6.94	6.33	-
CIP+AlexNet	80.69	23.46	16.21	15.14
OSS+AlexNet	92.13	34.11	25.43	24.67
ISS+AlexNet	93.28	29.39	21.90	20.48
CIP+VGG	80.69	29.80	20.12	18.99
ISS+VGG	93.93	39.13	28.65	27.24
CIP+CTCNet	80.69	21.56	12.14	11.27
OSS+CTCNet	93.29	30.66	21.31	21.59
ISS+CTCNet	**94.03**	24.13	**12.07**	**11.93**

To further evaluate the speed performance of the proposed CTCNet with different platforms, we implement CTCNet on a CPU platform, GPU platform and NPU platform. The CPU platform and GPU platform are used on the workstation described above. The NPU platform that we adopt in the experiment is the Atlas 200 platform. As shown in Table 3, when running CTCNet, the NPU platform has the highest processing speed, while the hardware platform with GPU can achieve almost the same efficiency. We also observe that even though the time consumed is doubled for the pure CPU platform, it is still acceptable for most clinical scenarios. This means that the proposed algorithm can be implemented on most mainstream platforms.

This paper uses data set to compare different cancer cell image detection networks, CTCNet has achieved slightly better performance than these networks. Moreover, combined with the ISS algorithm proposed in this paper, CTCNet can directly recognize CTCs in the whole image visual field, which improves the detection efficiency of CTCs in practical scene. The network proposed in this paper is not compared with the best performing network, but it exceeds two universal detection networks. What's more, it improves the detection accuracy and speed in the whole visual field of the CTC images.

Fig. 10 shows part of the test results by using the ISS+CTCNet. Fig. 10(a) to Fig. 10(d) detect false negative (FN) cells. Fig. 10(a) and Fig. 10(b) because of weak target information which confused with real ones; Fig. 10(c) shows overexposure leading to an unexpected background color, which leads to misjudgment; Fig. 10(d) shows a misjudged target in the boundary region, where the morphology of cells is difficult to distinguish. In Fig. 10(e), the algorithm missed a false positive cell, because the area of the cell mass was too large and the morphological characteristics were beyond the detection scope of CTCNet. In addition, in Fig. 10(f) and Fig. 10(g), large cells can be detected in most cases, and the size of the selection box can be adjusted adaptively. In Fig. 10(h), using an image contains no tumor cell. Fig. 10(i) to Fig. 10(l) show the generalization ability of the algorithm in different complex backgrounds. The target can be detected when there is large background interference (in Fig. 10(i) and Fig. 10(j)), unknown target interference (in Fig. 10(k)) and white blood cell interference (in Fig. 10(l)). Overall, the method proposed in this paper has the ability to adapt to different backgrounds, and it can also capture weak information. It has a good performance both in detection accuracy and speed.

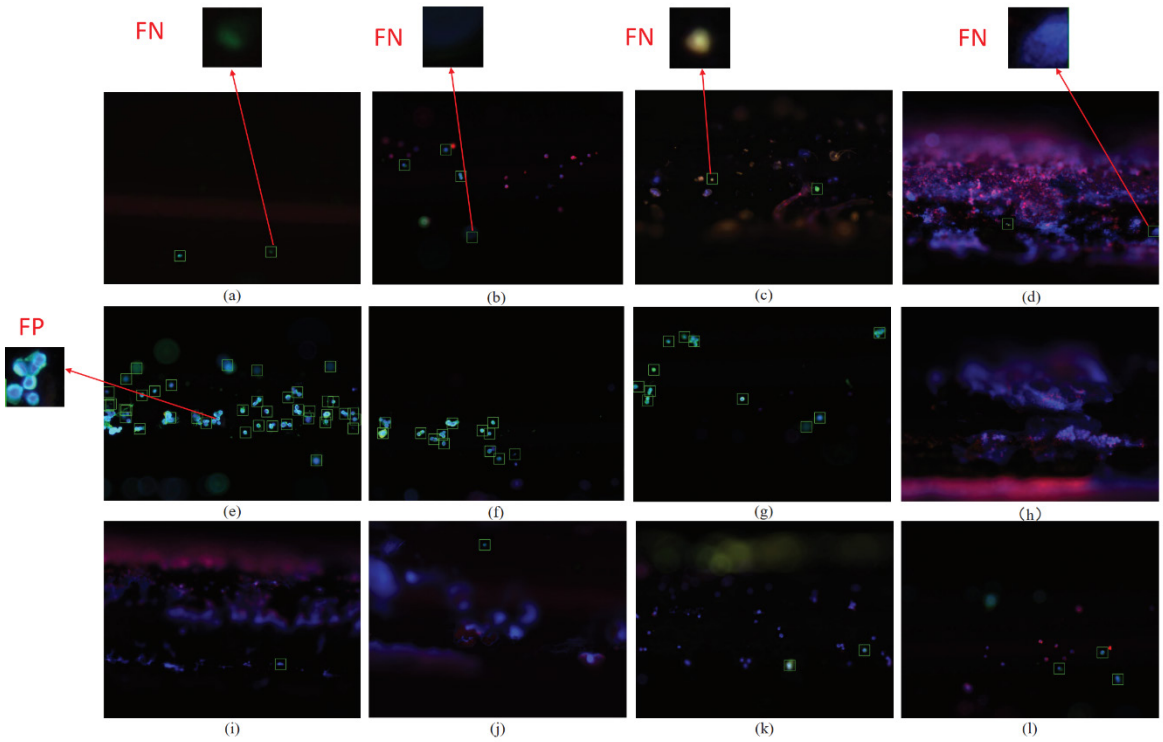

Fig. 10. Partial detection results of the method in this paper
(a) to (d) Figures with misjudgement; (e) Figure with missing target marked with a red box; (f) to (h) Figures with large cells and less background interference; (i) to (l) Figures with weak target signal and more background interference

5 Conclusion

This paper proposed an intelligent method to improve the accuracy and the speed of CTC cell detection. CTCNet adopts ISS to preprocess images and eliminate extra invalid candidate boxes. The proposed network has 7 layers and is optimized from AlexNet, combined with ISS, detection accuracy in clinical images can reach 94.03%. The proposed method can be implemented on various platforms (such as CPU, GPU, NPU), which accelerates the detection speed on the whole view of the CTC images.

Data is an important guarantee for training network, in the future, we plan to continuously update the CTC dataset by obtaining more clinical images. On the basis of the original model, we will continuously train and update the network on the new dataset. Meanwhile, region preselection affects the results of subsequent algorithms in two-stage object detection, thus we will continue to improve the candidate box extraction algorithm, expecting to thoroughly eliminate missing detection and further improve the accuracy of the CTCNet. For specific target recognition problems, we should pay more attention to the characteristics of the target signal [30]. We will first use some traditional signal processing methods to research the essential characteristics of CTC images. This inspires us to design area preselection algorithm from a more explanatory angle. Second, we hope to try various hardware acceleration platforms to realize off-line deployment of the algorithm as soon as possible. Finally, by continuing to expand our data set, we hope that a data set dedicated to CTC recognition will be established, which will summarize the existing datasets of cancer cell images to facilitate later research.

6 Acknowledgement

This work was supported in part by the National Natural Science Foundation of China (under Project 61906128). We thank LetPub (www.letpub.com) for its linguistic assistance during the preparation of this manuscript.

References

[1] J. Liu, S. Li, V.R. Bhethanabotla, Metal-enhanced immunofluorescence assays for detection of carcinoembryonic antigen, IEEE Sensors (2017) 1-3.

[2] C. Yeh, K. Su, Y. Lin, P. Shen, Using the newly microfluidic biosensor for carcinoembryonic antigen detection, IEEE Sensors (2014) 1866-1868.

[3] G. Haitao, C. Jiakun, T. Sheng, The establishment of detecting carbohydrate antigen 125 (CA125) with immunofluorescence chromatography, 2nd International Conference on Advanced Robotics and Mechatronics (ICARM) (2017) 184-188.

[4] K. Ding, C. Wang, B. Zhang, Y. Zhang, M. Guan, L. Cui, Y. Zhang, Y. Zeng, Z. Lin, F. Huang, Specific detection of alpha-fetoprotein using AlGaAs/GaAs high electron mobility transistors, IEEE Electron Device Letters 35(3)(2014) 333-335.

[5] J.S. de Bono, H.I. Scher, R.B. Montgomery, C. Parker, M.C. Miller, H. Tissing, G.V. Doyle, L.W. Terstappen, K.J. Pienta, D. Raghavan, Circulating tumor cells predict survival benefit from treatment in metastatic castrationresistant prostate cancer, Clinical Cancer Research 14(2008) 6302-6309.

[6] J. Tol, M. Koopman, M.C. Miller, A. Tibbe, A. Cats, G.J.M. Creemers, A.H. Vos, I.D. Nagtegaal, L.W.M.M. Terstappen, C.J.A. Punt, Circulating tumor cells early predict progression-free and overall survival in advanced colorectal cancer patients treated with chemotherapy and targeted agents, Annals of Oncology 21(2010) 1006-1012.

[7] J. W. Xu, T. D. Pham, X. Zhou, A double thresholding method for cancer stem cell detection, 7th International Symposium on Image and Signal Processing and Analysis (ISPA) (2011) 695-699.

[8] Y. Xu, J. Zhu, E. Chang, Z. Tu, Multiple clustered instance learning for histopathology cancer image classification, segmentation and clustering, IEEE Conference on Computer Vision and Pattern Recognition (2012) 964-971.

[9] S.H. Lewis, A. Dong, Detection of breast tumor candidates using marker-controlled watershed segmentation and morphological analysis, IEEE Southwest Symposium on Image Analysis and Interpretation (2012) 1-4.

[10] O. Oguz, C. Muenzenmayer, T. Wittenberg, A. Uner, A.E. Cetin, R.C. Atalay, Detection of cancer stem cells in microscopic images by using region covariance and codifference method, International Workshop on Computational Intelligence for Multimedia Understanding (IWCIM) (2015) 1-5.

[11] H. Alquran, I.A. Qasmieh, A.M. Alqudah, S. Alhammouri, E. Alawneh, A. Abughazaleh, F. Hasayen, The melanoma skin cancer detection and classification using support vector machine, IEEE Jordan Conference on Applied Electrical Engineering and Computing Technologies (2017) 1-5.

[12] A. Khosravi, J. Addeh, J. Ganjipour, Breast cancer detection using BA-BP based neural networks and efficient features, 7th Iranian Conference on Machine Vision and Image Processing (2011) 1-6.

[13] Z. Wang, C. Liu, D. Cheng, L. Wang, X. Yang, K. Cheng, Automated detection of clinically significant prostate cancer in mp-MRI images based on an end-to-end deep neural network, IEEE Transactions on Medical Imaging 37(5)(2018) 1127-1139.

[14] H. Nasir Khan, A.R. Shahid, B. Raza, A.H. Dar, H. Alquhayz, Multi-View feature fusion based four views model for mammogram classification using convolutional neural network, IEEE Access 7(2019) 165724-165733.

[15] N. Mohanapriya, B. Kalaavathi, T.S. Kuamr, Lung tumor classification and detection from CT scan images using deep convolutional neural networks, International Conference on Computational Intelligence and Knowledge Economy (ICCIKE) (2019) 800-805.

[16] L. Zhang, Le Lu, I. Nogues, R.M. Summers, S. Liu, J. Yao, Deeppap: Deep convolutional networks for cervical cell classification, IEEE Journal of Biomedical and Health Informatics 21(6)(2017) 1633-1643.

[17] S. Nagrath, L.V. Sequist, S. Maheswaran, D.W. Bell, D. Irimia, L. Ulkus, M.R. Smith, E.L. Kwak, S. Digumarthy, A. Muzikansky, P. Ryan, U.J. Balis, R.G. Tompkins, D.A. Haber, M. Toner, Isolation of rare circulating tumour cells in cancer patients by microchip technology, Nature 450(2007) 1235-1239.

[18] C. Yang, N. Zhang, S. Wang, D. Shi, C. Zhang, K. Liu, B. Xiong, Wedge-shaped microfluidic chip for circulating tumor cells isolation and its clinical significance in gastric cancer, Journal of Translational Medicine 16(2018).

[19] Y. Mao, Z. Yin, J.M. Schober, Iteratively training classifiers for circulating tumor cell detection, IEEE 12th International Symposium on Biomedical Imaging (ISBI) (2015) 190-194.

[20] C.-M. Svensson, S. Krusekopf, J. Lucke, M. Tilo Figge, Automated classification of circulating tumor cells and the impact of interobsever variability on classifier training and performance, Advances in Computational Immunology (2015) 1-9.

[21] T.B. Lannin, F.I. Thege, B.J. Kirby, Comparison and optimization of machine learning methods for automated classifcation of circulating tumor cells, Cytometry A 89(2016) 922-931.

[22] C.-M. Svensson, S. Krusekopf, J. Lucke, M.T. Figge, Automated detection of circulating tumor cells with naive Bayesian classifers, Cytometry A 85(2014) 501-511.

[23] Y. Mao, Z. Yin, J. Schober, A deep convolutional neural network trained on representative samples for circulating tumor cell detection, IEEE Winter Conference on Applications of Computer Vision (WACV) (2016) 1-6.

[24] L.L. Zeune, Y.E. Boink, G. van Dalum, A. Nanou, S. de Wit, K.C. Andree, J.F. Swennenhuis, S.A. van Gils, L.W.M. M. Terstappen, C. Brune, Deep learning of circulating tumour cells, Nature Machine Intelligence 2(2020).

[25] B. He, Q. Lu, J. Lang, H. Yu, C. Peng, P. Bing, S. Li, Q. Zhou, Y. Liang, G. Tian, A new method for CTC images recog-

nition based on machine learning, Frontiers in Bioengineering and Biotechnology 8(2020) 1-10.
[26] T. Fukagai, K. Maeda, S. Tanabe, K. Shirahata, Y. Tomita, A. Ike, A. Nakagawa, Speed-up of object detection neural network with GPU, 25th IEEE International Conference on Image Processing (ICIP) (2018) 301-305.
[27] C. Lammie, A. Olsen, T. Carrick, M. Rahimi Azghadi, Low-power and high-speed deep FPGA inference engines for weed classification at the edge, IEEE Access 7(2019) 51171-51184.
[28] W. Li, J. Li, K.V. Sarma, K.C. Ho, S. Shen, B.S. Knudsen, A. Gertych, C.W. Arnold, Path R-CNN for prostate cancer diagnosis and gleason grading of histological images, IEEE Transactions on Medical Imaging 38(4)(2019) 945-954.
[29] W. Zhang, S. Wang, S. Thachan, J. Chen, Y. Qian, Deconv R-CNN for small object detection on remote sensing images, IEEE International Geoscience and Remote Sensing Symposium (2018) 2483-2486.
[30] J. Jiang, T. Shi, M. Huang, Z. Xiao, Multi-scale spectral feature extraction for underwater acoustic target recognition, Measurement 166(2020).